Journal of Scientific Computing, Vol. 14, No. 2, 1999

Incident Wave Source for Finite-Difference Time-Domain Computation of Electromagnetic Scattering for Objects Embedded in Layered Dispersive Media

Michael S. Yeung[1]

Received April 6, 1999

An incident wave source for finite-difference time-domain (FDTD) computation of electromagnetic scattering involving layered dispersive media is described. The method is based on the decomposition of an arbitrary incident wave into its frequency components and computing the corresponding steady-state fields in the FDTD lattice analytically. The wave source can in principle generate an incident wave obeying the dispersion relations and reflection and transmission relations of the FDTD lattice exactly. Numerical results show that, in practical computation, the accuracy of the generated incident wave is limited by FFT aliasing error occurring during waveform synthesis.

KEY WORDS: Electromagnetic scattering; finite-difference time-domain computation; dispersive media.

1. INTRODUCTION

In many applications, it is often necessary to compute the electromagnetic scattering by an object embedded in a layered medium due to an incident wave originating from a distant source. When the finite-difference time-domain (FDTD) method is used for such a computation, the computational domain is truncated to a finite size and special boundary conditions are applied on the domain boundaries to absorb the outgoing waves. Also, the incident fields must be known at all time steps throughout the computational domain, or over a closed surface enclosing the scattering object, in order to apply the necessary excitation. In the former case, referred to as

[1] Department of Manufacturing Engineering, Boston University, 15 St. Mary's Street, Boston, Massachusetts 02215. E-mail: myeung@bu.edu.

0885-7474/99/0600-0121$16.00/0

the scattered-field formulation, the FDTD method is applied to time-step only the *scattered* electric and magnetic fields throughout the computational domain. The total fields are obtained by adding the known incident fields to the FDTD computed scattered fields. In the latter case, referred to as the total-field formulation, the computational domain is divided into two regions by a fictitious surface enclosing the scattering object. In the interior, total-field region, the FDTD method is applied to the total electric and magnetic fields, while in the exterior, scattered-field region, the FDTD method is applied to the scattered fields only.

For accurate results, the incident fields used to excite the FDTD computational domain should be the fields that would propagate in the FDTD lattice, rather than those that would propagate in physical space, in the absence of the scattering object. In the scattered-field formulation, the incident and scattered fields may nearly cancel one another in certain regions of the computational domain, such as the interior of a shielded cavity or the back side of an absorbing layer of material. To minimize differencing noise in the computation of the total fields in such regions, the incident fields obeying the same dispersion relations as the FDTD computed scattered fields must be used. In the total-field formulation, the incident fields applied to the fictitious surface enclosing the scattering object are allowed to propagate across the interior FDTD region. However, in order for the fields propagating across the interior region by FDTD to be cancelled exactly by the incident fields applied to the fictitious surface as the former fields attempt to pass out of the latter surface, the incident fields applied to the latter surface must obey the same dispersion relations as the FDTD computed fields in the interior region.

To generate the incident fields obeying the dispersion relations of the FDTD lattice, one approach is to set up an auxiliary one-dimensional FDTD lattice having the same dispersion relations as the three-dimensional FDTD lattice in the direction of propagation of the incident wave [Holland and Williams (1983)]. The required incident fields are obtained as solution to the auxiliary one-dimensional problem. However, this approach is straightforward only when the incident wave propagates along a coordinate axis. In the case of off-axis propagation, the parameters of the auxiliary one-dimensional FDTD lattice would have to be frequency dependent, in order to match the dispersion relations of the three-dimensional FDTD lattice exactly at *all* the frequencies contained in a finite-duration incident pulse. Furthermore, in the case of a layered three-dimensional FDTD lattice, the auxiliary one-dimensional FDTD lattice would have to possess the same reflection and transmission coefficients at the boundaries between adjacent materials as the three-dimensional lattice, at all the frequencies contained in the incident pulse. It is not obvious how such an

auxiliary one-dimensional FDTD lattice could be constructed for the general case of off-axis incidence in a layered three-dimensional FDTD lattice.

In this paper, the incident fields obeying the dispersion relations of a layered, dispersive three-dimensional FDTD lattice are generated by decomposing the incident pulse into its frequency components and computing the steady-state fields in the three-dimensional lattice due to each frequency component analytically, by solving the corresponding steady-state FDTD equations. The incident waveform at each point of excitation in the computational domain is then obtained by Fast Fourier Transform (FFT) of the computed steady-state fields at that point. The incident waveforms so obtained obey the correct dispersion relations and reflection and transmission relations of the layered three-dimensional FDTD lattice, for arbitrary direction of incidence and frequency content of the incident pulse. These incident waveforms are thus suitable for accurate FDTD computation using the scattered-field or total-field formulation.

The computation of the steady-state fields in a layered, dispersive FDTD lattice is discussed in Section 2. The method described is numerically stable for propagating *and* evanescent waves in an FDTD lattice consisting of an arbitrary number of lossy, dispersive layers. Numerical results are presented in Section 3 to demonstrate the accuracy with which the incident fields can be generated by the wave source.

2. STEADY-STATE FIELDS IN A LAYERED FDTD LATTICE

An arbitrary incident wave propagating in the uppermost layer of a layered medium can be represented by a superposition of plane waves of different frequencies, polarizations and directions of propagation. It is only necessary to consider the steady-state fields in the layered FDTD lattice due to a single incident plane wave of frequency ω, polarization $\mathbf{E}^{\text{inc}}$ and transverse wavevector (k_x, k_y). The results for an arbitrary incident wave are obtained by superposition.

2.1. Dispersion Relations

The geometry of an FDTD lattice consisting of $M+1$ homogeneous layers separated by M planar interfaces is shown in Fig. 1. The FDTD cells are constrained to have the same widths (Δ_x, Δ_y) in the x and y directions, but their heights Δ_z^m in the z direction may vary with the layer index m. In the standard Yee algorithm [see Yee (1966)], an FDTD cell labeled by spatial indices (i, j, k), as shown in Fig. 2, is associated with six field components, $E^n_{x,\, i+1/2,\, j,\, k}$, $E^n_{y,\, i,\, j+1/2,\, k}$, $E^n_{z,\, i,\, j,\, k+1/2}$, $H^{n+1/2}_{x,\, i,\, j+1/2,\, k+1/2}$, $H^{n+1/2}_{y,\, i+1/2,\, j,\, k+1/2}$, $H^{n+1/2}_{z,\, i+1/2,\, j+1/2,\, k}$, where n is the temporal index. In the

steady state, the wave in layer m due to an incident plane wave of frequency ω and transverse wavevector (k_x, k_y) can be written as the sum of a downward propagating and an upward propagating plane wave in the FDTD lattice,

$$\begin{bmatrix} E^n_{x,\,i+1/2,\,j,\,k} \\ E^n_{y,\,i,\,j+1/2,\,k} \\ E^n_{z,\,i,\,j,\,k+1/2} \\ H^{n+1/2}_{x,\,i,\,j+1/2,\,k+1/2} \\ H^{n+1/2}_{y,\,i+1/2,\,j,\,k+1/2} \\ H^{n+1/2}_{z,\,i+1/2,\,j+1/2,\,k} \end{bmatrix} = \begin{bmatrix} E^m_x \\ E^m_y \\ E^m_z \\ H^m_x \\ H^m_y \\ H^m_z \end{bmatrix} e^{\hat{\jmath}\omega n\,\Delta t - \hat{\jmath}(ik_x\Delta_x + jk_y\Delta_y - kk^m_z\Delta^m_z)}$$

$$+ \begin{bmatrix} E^{rm}_x \\ E^{rm}_y \\ E^{rm}_z \\ H^{rm}_x \\ H^{rm}_y \\ H^{rm}_z \end{bmatrix} e^{\hat{\jmath}\omega n\,\Delta t - \hat{\jmath}(ik_x\Delta_x + jk_y\Delta_y + kk^m_z\Delta^m_z)} \tag{2.1}$$

where $\hat{\jmath} = \sqrt{-1}$ is the unit imaginary number, to be distinguished from the spatial index j, and k^m_z is the z component of the wavevector in layer m. The latter is determined by the numerical dispersion relation for layer m. Furthermore, not all of the field coefficients $(E^m_x, E^m_y, E^m_z, H^m_x, H^m_y, H^m_z)$, or $(E^{rm}_x, E^{rm}_y, E^{rm}_z, H^{rm}_x, H^{rm}_y, H^{rm}_z)$, in this equation are independent. To see this, consider the downward propagating plane wave represented by the first term on the right-hand side (RHS) of Eq. (2.1). The FDTD equations for this plane wave in layer m can be written in accordance with the Yee algorithm as

$$\varepsilon_m E^m_x(\gamma_m e^{\hat{\jmath}\omega\,\Delta t} - \beta_m) = \Delta t\left[\frac{1 - e^{\hat{\jmath}k_y\Delta_y}}{\Delta_y} H^m_z - \frac{1 - e^{-\hat{\jmath}k^m_z\Delta^m_z}}{\Delta^m_z} H^m_y\right] \tag{2.2}$$

$$\varepsilon_m E^m_y(\gamma_m e^{\hat{\jmath}\omega\,\Delta t} - \beta_m) = \Delta t\left[\frac{1 - e^{-\hat{\jmath}k^m_z\Delta^m_z}}{\Delta^m_z} H^m_x - \frac{1 - e^{\hat{\jmath}k_x\Delta_x}}{\Delta_x} H^m_z\right] \tag{2.3}$$

$$\varepsilon_m E^m_z(\gamma_m e^{\hat{\jmath}\omega\,\Delta t} - \beta_m) = \Delta t\left[\frac{1 - e^{\hat{\jmath}k_x\Delta_x}}{\Delta_x} H^m_y - \frac{1 - e^{\hat{\jmath}k_y\Delta_y}}{\Delta_y} H^m_x\right] \tag{2.4}$$

$$\mu_m H_x^m(1-e^{-j\omega\Delta t}) = -\Delta t\left[\frac{e^{-jk_y\Delta_y}-1}{\Delta_y}E_z^m - \frac{e^{jk_z^m\Delta_z^m}-1}{\Delta_z^m}E_y^m\right] \tag{2.5}$$

$$\mu_m H_y^m(1-e^{-j\omega\Delta t}) = -\Delta t\left[\frac{e^{jk_z^m\Delta_z^m}-1}{\Delta_z^m}E_x^m - \frac{e^{-jk_x\Delta_x}-1}{\Delta_x}E_z^m\right] \tag{2.6}$$

$$\mu_m H_z^m(1-e^{-j\omega\Delta t}) = -\Delta t\left[\frac{e^{-jk_x\Delta_x}-1}{\Delta_x}E_y^m - \frac{e^{-jk_y\Delta_y}-1}{\Delta_y}E_x^m\right] \tag{2.7}$$

where ε_m, μ_m, γ_m, and β_m are parameters characterizing layer m. These parameters are given in the Appendix for three commonly used, lossy, dispersive material models.

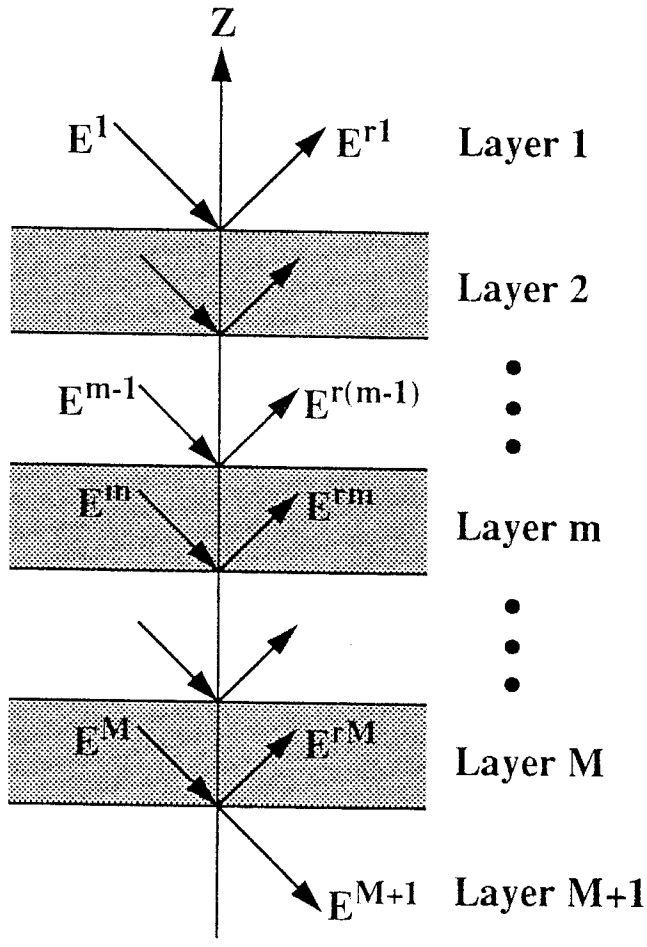

Fig. 1. Layered FDTD lattice consisting of $M+1$ homogeneous layers separated by M planar interfaces.

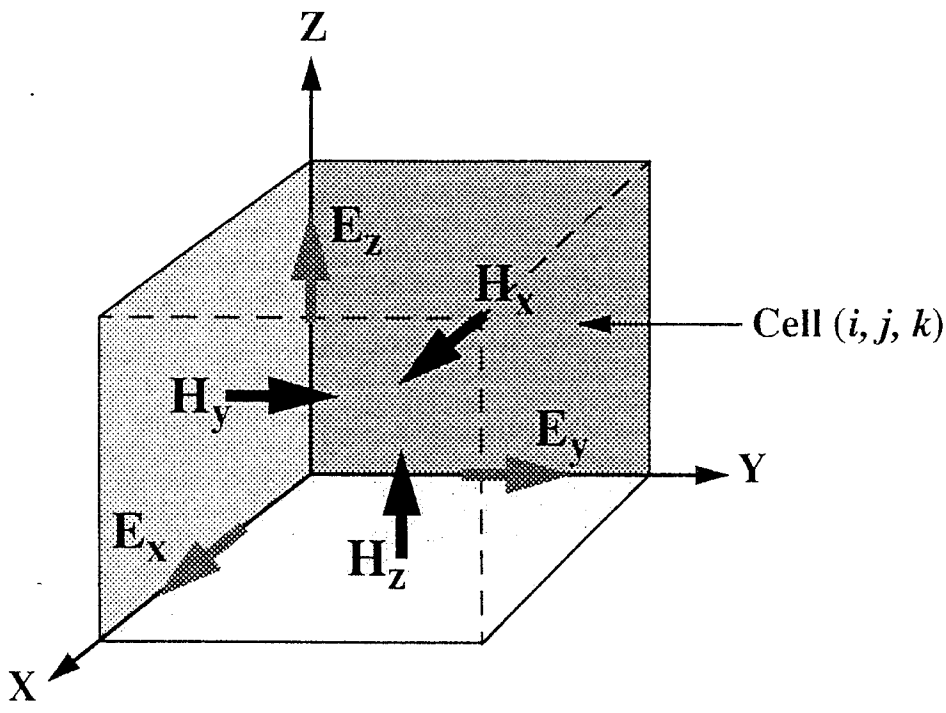

Fig. 2. FDTD cell with its associated electric and magnetic field components. The electric field nodes lie at the centers of the edges and the magnetic field nodes lie at the center of the faces.

By substituting Eqs. (2.2)–(2.4) into Eqs. (2.5)–(2.7), one derives the numerical dispersion relation for layer m:

$$\left[\frac{\sin(k_x \Delta_x/2)}{\Delta_x}\right]^2 + \left[\frac{\sin(k_y \Delta_y/2)}{\Delta_y}\right]^2 + \left[\frac{\sin(k_z^m \Delta_z^m/2)}{\Delta_z^m}\right]^2$$
$$= \mu_m \varepsilon_m \gamma_m \left[\frac{\sin(\omega \Delta t/2)}{\Delta t}\right]^2 - \frac{\mu_m \varepsilon_m (\gamma_m - \beta_m)}{4(\Delta t)^2}(1 - e^{-j\omega \Delta t}) \tag{2.8}$$

This relation allows k_z^m to be solved in terms of the transverse wavevector (k_x, k_y) of the incident plane wave.

From Eqs. (2.2)–(2.4), one readily derives the relationship

$$(1 - e^{-jk_x \Delta_x})\, \Delta_y \Delta_z^m E_x^m + (1 - e^{-jk_y \Delta_y})\, \Delta_x \Delta_z^m E_y^m$$
$$+ (1 - e^{-jk_z^m \Delta_z^m})\, \Delta_x \Delta_y E_z^m = 0 \tag{2.9}$$

This relationship allows E_z^m to be expressed in terms of (E_x^m, E_y^m). Then, using Eqs. (2.5)–(2.7), the magnetic field coefficients (H_x^m, H_y^m, H_z^m) can also be expressed in terms of (E_x^m, E_y^m). This shows that only two of the six field coefficients $(E_x^m, E_y^m, E_z^m, H_x^m, H_y^m, H_z^m)$ of the downward propagating

plane wave are independent. Similarly, only two of the six field coefficients $(E_x^{rm}, E_y^{rm}, E_z^{rm}, H_x^{rm}, H_y^{rm}, H_z^{rm})$ of the upward propagating plane wave are independent. Thus, the fields in layer m, as given by Eq. (2.1) are completely determined by four independent coefficients, which may be chosen as $(E_x^m, E_y^m, E_x^{rm}, E_y^{rm})$.

2.2. Fields in the FDTD Lattice

To find the independent coefficients $(E_x^m, E_y^m, E_x^{rm}, E_y^{rm})$ for all layers m, one can use the approach of matrix optics. Instead of applying the boundary condition of continuity of the tangential field components across each planar interface as in matrix optics, here one applies the FDTD equations to the magnetic and electric field nodes situated in the immediate vicinity of each planar interface. For simplicity, each planar interface is assumed to coincide with a cell face. This situation can always be realized by choosing the FDTD cell heights Δ_z^m in such a way that each layer contains an integral number of FDTD cells in the z direction.

The interface between layers m and $m+1$, which coincides with the bottom face of an FDTD cell (i, j, k) with $k = N_m$, is illustrated in Fig. 3. The magnetic field components at the two magnetic field nodes immediately above the interface are given by Eq. (2.1) with $k = N_m$. Thus, for these nodes, $H^{n+1/2}_{x,\,i,\,j+1/2,\,k+1/2} = [H_x^m \phi_m^{(+)} + H_x^{rm} \phi_m^{(-)}]\, e^{j\omega n\,\Delta t - j(ik_x \Delta_x + jk_y \Delta_y)}$, and similarly for $H^{n+1/2}_{y,\,i+1/2,\,j,\,k+1/2}$, where

$$\phi_m^{(\pm)} = e^{\pm jN_m k_z^m \Delta_z^m} \tag{2.10}$$

The magnetic field components at the two magnetic field nodes immediately below the interface are given by Eq. (2.1) with superscripts m replaced by $(m+1)$ and $k = (N_m - 1)$. Thus, for these nodes, $H^{n+1/2}_{x,\,i,\,j+1/2,\,k+1/2} = [H_x^{m+1} \psi_m^{(+)} + H_x^{r(m+1)} \psi_m^{(-)}]\, e^{j\omega n\,\Delta t - j(ik_x \Delta_x + jk_y \Delta_y)}$, and similarly for $H^{n+1/2}_{y,\,i+1/2,\,j,\,k+1/2}$, where

$$\psi_m^{(\pm)} = e^{\pm j(N_m - 1) k_z^{m+1} \Delta_z^{m+1}} \tag{2.11}$$

However the field components at the electric and magnetic field nodes lying *on* the interface are not given by Eq. (2.1), since the former field components obey interfacial FDTD equations rather than the FDTD equations (2.2), (2.3), and (2.7) for the interior of a layer. Instead, the field components at the interfacial nodes are assumed to have the form

$$\begin{bmatrix} E^n_{x,\,i+1/2,\,j,\,N_m} \\ E^n_{y,\,i,\,j+1/2,\,N_m} \\ H^{n+1/2}_{z,\,i+1/2,\,j+1/2,\,N_m} \end{bmatrix} = \begin{bmatrix} F^m \\ G^m \\ Q^m \end{bmatrix} e^{j\omega n\,\Delta t - j(ik_x \Delta_x + jk_y \Delta_y)} \tag{2.12}$$

where k has been set equal to N_m on the left-hand side (LHS) of this equation. By applying the contour-path method [Taflove (1995)] to the interfacial nodes, one derives the interfacial FDTD equations for these nodes,

$$F^m \Gamma^m = \Delta t \left[\frac{\Delta_z^m + \Delta_z^{m+1}}{2\Delta_y} (1 - e^{\hat{\jmath} k_y \Delta_y}) Q^m - H_y^m \phi_m^{(+)} - H_y^{rm} \phi_m^{(-)} + H_y^{m+1} \psi_m^{(+)} + H_y^{r(m+1)} \psi_m^{(-)} \right] \tag{2.13}$$

$$G^m \Gamma^m = -\Delta t \left[\frac{\Delta_z^m + \Delta_z^{m+1}}{2\Delta_x} (1 - e^{\hat{\jmath} k_x \Delta_x}) Q^m - H_x^m \phi_m^{(+)} - H_x^{rm} \phi_m^{(-)} + H_x^{m+1} \psi_m^{(+)} + H_x^{r(m+1)} \psi_m^{(-)} \right] \tag{2.14}$$

$$Q^m (1 - e^{-\hat{\jmath}\omega \Delta t}) = \frac{\Delta t}{\mu_m} \left[\frac{e^{-\hat{\jmath} k_y \Delta_y} - 1}{\Delta_y} F^m - \frac{e^{-\hat{\jmath} k_x \Delta_x} - 1}{\Delta_x} G^m \right] \tag{2.15}$$

where

$$\Gamma^m = \frac{\varepsilon_m \Delta_z^m}{2} (\gamma_m e^{\hat{\jmath}\omega \Delta t} - \beta_m) + \frac{\varepsilon_{m+1} \Delta_z^{m+1}}{2} (\gamma_{m+1} e^{\hat{\jmath}\omega \Delta t} - \beta_{m+1}) \tag{2.16}$$

The unknowns in these equations are $(F^m, G^m, Q^m, E_x^m, E_y^m, E_x^{rm}, E_y^{rm})$, assuming that $(E_x^{m+1}, E_y^{m+1}, E_x^{r(m+1)}, E_y^{r(m+1)})$ are known. To solve for the former set of seven unknowns, one needs four more equations besides Eqs. (2.13) to (2.15). These are the FDTD equations for the four magnetic field nodes immediately above or below the interface, as shown in Fig. 3. Using Eq. (2.1) with the appropriate indices m and k, these equations can be written as

$$[H_x^m \phi_m^{(+)} + H_x^{rm} \phi_m^{(-)}](1 - e^{-\hat{\jmath}\omega \Delta t}) = -\frac{\Delta t}{\mu_m} \left[\frac{e^{-\hat{\jmath} k_y \Delta_y} - 1}{\Delta_y} (E_z^m \phi_m^{(+)} + E_z^{rm} \phi_m^{(-)}) - \frac{1}{\Delta_z^m} (E_y^m \phi_m^{(+)} e^{\hat{\jmath} k_z^m \Delta_z^m} + E_y^{rm} \phi_m^{(-)} e^{-\hat{\jmath} k_z^m \Delta_z^m} - G^m) \right] \tag{2.17}$$

$$[H_y^m \phi_m^{(+)} + H_y^{rm} \phi_m^{(-)}](1 - e^{-\hat{\jmath}\omega \Delta t}) = \frac{\Delta t}{\mu_m} \left[\frac{e^{-\hat{\jmath} k_x \Delta_x} - 1}{\Delta_x} (E_z^m \phi_m^{(+)} + E_z^{rm} \phi_m^{(-)}) - \frac{1}{\Delta_z^m} (E_x^m \phi_m^{(+)} e^{\hat{\jmath} k_z^m \Delta_z^m} + E_x^{rm} \phi_m^{(-)} e^{-\hat{\jmath} k_z^m \Delta_z^m} - F^m) \right] \tag{2.18}$$

his equa-
e interfa-
nodes,

$^{n}\phi_m^{(-)}$

(2.13)

$H_x^{rm}\phi_m^{(-)}$

(2.14)

(2.15)

(2.16)

E_x^{rm}, E_y^{rm}),
solve for
ns besides
magnetic
in Fig. 3.
ations can

(2.17)

(2.18)

$$[H_x^{m+1}\psi_m^{(+)} + H_x^{r(m+1)}\psi_m^{(-)}](1 - e^{-j\omega\Delta t})$$
$$= -\frac{\Delta t}{\mu_{m+1}}\left[\frac{e^{-jk_y\Delta_y} - 1}{\Delta_y}(E_z^{m+1}\psi_m^{(+)} + E_z^{r(m+1)}\psi_m^{(-)})\right.$$
$$\left. + \frac{1}{\Delta_z^{m+1}}(E_y^{m+1}\psi_m^{(+)} + E_y^{r(m+1)}\psi_m^{(-)} - G^m)\right] \quad (2.19)$$

$$[H_y^{m+1}\psi_m^{(+)} + H_y^{r(m+1)}\psi_m^{(-)}](1 - e^{-j\omega\Delta t})$$
$$= \frac{\Delta t}{\mu_{m+1}}\left[\frac{e^{-jk_x\Delta_x} - 1}{\Delta_x}(E_z^{m+1}\psi_m^{(+)} + E_z^{r(m+1)}\psi_m^{(-)})\right.$$
$$\left. + \frac{1}{\Delta_z^{m+1}}(E_x^{m+1}\psi_m^{(+)} + E_x^{r(m+1)}\psi_m^{(-)} - F^m)\right] \quad (2.20)$$

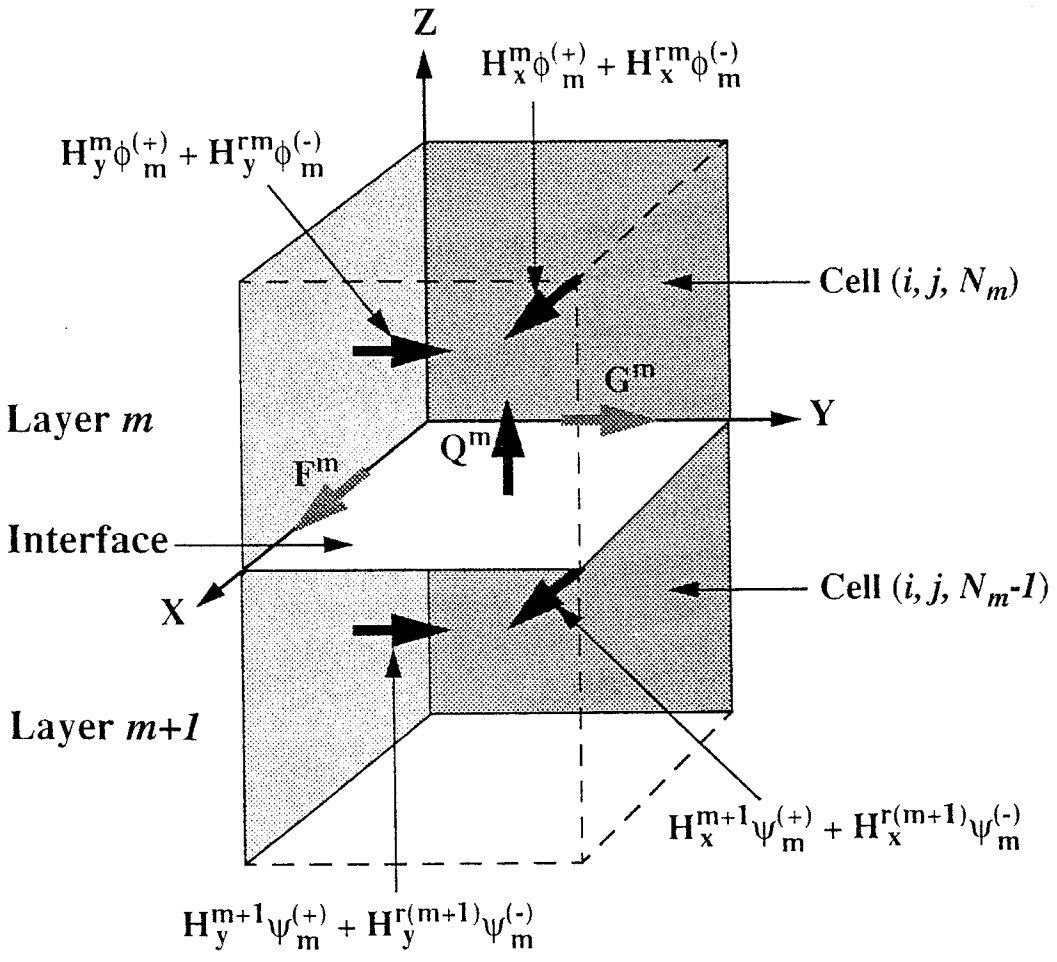

Fig. 3. Interface between layers m and $m+1$ separating FDTD cells with $k = N_m$ from those with $k = N_m - 1$.

To simplify the notation, it is convenient to introduce the following quantities:

$$\eta_x^m = \frac{\Delta t(e^{j k_x \Delta_x} - 1)}{\mu_m \Delta_x} \tag{2.21}$$

$$\eta_y^m = \frac{\Delta t(e^{j k_y \Delta_y} - 1)}{\mu_m \Delta_y} \tag{2.22}$$

$$\eta_z^{m(\pm)} = \frac{\Delta t(e^{\pm j k_z^m \Delta_z^m} - 1)}{\mu_m \Delta_z^m} \tag{2.23}$$

$$A_m^{(\pm)} = \frac{\eta_x^m \eta_y^m e^{-j k_x \Delta_x}}{\eta_z^{m(\pm)} e^{\mp j k_z^m \Delta_z^m}} \tag{2.24}$$

$$B_m^{(\pm)} = \eta_z^{m(\pm)} + \frac{(\eta_y^m)^2 e^{-j k_y \Delta_y}}{\eta_z^{m(\pm)} e^{\mp j k_z^m \Delta_z^m}} \tag{2.25}$$

$$C_m^{(\pm)} = \eta_z^{m(\pm)} + \frac{(\eta_x^m)^2 e^{-j k_x \Delta_x}}{\eta_z^{m(\pm)} e^{\mp j k_z^m \Delta_z^m}} \tag{2.26}$$

$$D_m^{(\pm)} = \frac{\eta_x^m \eta_y^m e^{-j k_y \Delta_y}}{\eta_z^{m(\pm)} e^{\mp j k_z^m \Delta_z^m}} \tag{2.27}$$

By substituting Eq. (2.15) into Eqs. (2.13) and (2.14) and using Eqs. (2.5)–(2.7) and (2.9), one obtains

$$\begin{bmatrix} F^m \\ G^m \end{bmatrix} = \begin{bmatrix} R_m^{(+)} & S_m^{(+)} & R_m^{(-)} & S_m^{(-)} \\ U_m^{(+)} & V_m^{(+)} & U_m^{(-)} & V_m^{(-)} \end{bmatrix} \begin{bmatrix} E_x^m \phi_m^{(+)} \\ E_y^m \phi_m^{(+)} \\ E_x^{rm} \phi_m^{(-)} \\ E_y^{rm} \phi_m^{(-)} \end{bmatrix}$$

$$- \begin{bmatrix} R_{m+1}^{(+)} & S_{m+1}^{(+)} & R_{m+1}^{(-)} & S_{m+1}^{(-)} \\ U_{m+1}^{(+)} & V_{m+1}^{(+)} & U_{m+1}^{(-)} & V_{m+1}^{(-)} \end{bmatrix} \begin{bmatrix} E_x^{m+1} \psi_m^{(+)} \\ E_y^{m+1} \psi_m^{(+)} \\ E_x^{r(m+1)} \psi_m^{(-)} \\ E_y^{r(m+1)} \psi_m^{(-)} \end{bmatrix} \tag{2.28}$$

where

$$\begin{bmatrix} R_m^{(\pm)} & S_m^{(\pm)} \\ U_m^{(\pm)} & V_m^{(\pm)} \end{bmatrix} = \Delta t \begin{bmatrix} W_{11} & W_{12} \\ W_{21} & W_{22} \end{bmatrix}^{-1} \begin{bmatrix} C_m^{(\pm)} & D_m^{(\pm)} \\ A_m^{(\pm)} & B_m^{(\pm)} \end{bmatrix} \tag{2.29}$$

llowing

(2.21)

(2.22)

(2.23)

(2.24)

(2.25)

(2.26)

(2.27)

nd using

and

$$W_{11} = \Gamma^m(1 - e^{-j\omega \Delta t}) - \mu_m \left(\frac{\Delta_z^m + \Delta_z^{m+1}}{2} \right) (\eta_y^m)^2 \, e^{-jk_y \Delta_y} \tag{2.30}$$

$$W_{12} = \mu_m \left(\frac{\Delta_z^m + \Delta_z^{m+1}}{2} \right) \eta_x^m \eta_y^m e^{-jk_y \Delta_y} \tag{2.31}$$

$$W_{21} = \mu_m \left(\frac{\Delta_z^m + \Delta_z^{m+1}}{2} \right) \eta_x^m \eta_y^m e^{-jk_x \Delta_x} \tag{2.32}$$

$$W_{22} = \Gamma^m(1 - e^{-j\omega \Delta t}) - \mu_m \left(\frac{\Delta_z^m + \Delta_z^{m+1}}{2} \right) (\eta_x^m)^2 \, e^{-jk_x \Delta_x} \tag{2.33}$$

Finally, by substituting Eq. (2.28) into Eqs. (2.17)–(2.20), the matrix-optics relationship between $(E_x^m, E_y^m, E_x^{rm}, E_y^{rm})$ and $(E_x^{m+1}, E_y^{m+1}, E_x^{r(m+1)}, E_y^{r(m+1)})$ is obtained:

$$\begin{bmatrix} E_x^m \phi_m^{(+)} \\ E_y^m \phi_m^{(+)} \\ E_x^{rm} \phi_m^{(-)} \\ E_y^{rm} \phi_m^{(-)} \end{bmatrix} = [A_m]^{-1} [B_m] \begin{bmatrix} E_x^{m+1} \psi_m^{(+)} \\ E_y^{m+1} \psi_m^{(+)} \\ E_x^{r(m+1)} \psi_m^{(-)} \\ E_y^{r(m+1)} \psi_m^{(-)} \end{bmatrix} \tag{2.34}$$

where $[A_m]$ and $[B_m]$ are 4×4 matrices,

$$[A_m] = \begin{bmatrix} A_m^{(+)} + \eta_y^m P_m^{(+)} + \zeta_m U_m^{(+)} & B_m^{(+)} + \eta_y^m Q_m^{(+)} - \zeta_m e^{jk_z^m \Delta_z^m} + \zeta_m V_m^{(+)} & A_m^{(-)} + \eta_y^m P_m^{(-)} + \zeta_m U_m^{(-)} & B_m^{(-)} + \eta_y^m Q_m^{(-)} - \zeta_m e^{-jk_z^m \Delta_z^m} + \zeta_m V_m^{(-)} \\ -C_m^{(+)} - \eta_x^m P_m^{(+)} + \zeta_m e^{jk_z^m \Delta_z^m} - \zeta_m R_m^{(+)} & -D_m^{(+)} - \eta_x^m Q_m^{(+)} - \zeta_m S_m^{(+)} & -C_m^{(-)} - \eta_x^m P_m^{(-)} + \zeta_m e^{-jk_z^m \Delta_z^m} - \zeta_m R_m^{(-)} & -D_m^{(-)} - \eta_x^m Q_m^{(-)} - \zeta_m S_m^{(-)} \\ -\zeta_{m+1} U_m^{(+)} & -\zeta_{m+1} V_m^{(+)} & -\zeta_{m+1} U_m^{(-)} & -\zeta_{m+1} V_m^{(-)} \\ \zeta_{m+1} R_m^{(+)} & \zeta_{m+1} S_m^{(+)} & \zeta_{m+1} R_m^{(-)} & \zeta_{m+1} S_m^{(-)} \end{bmatrix} \tag{2.35}$$

(2.28)

(2.29)

$$[B_m]=\begin{bmatrix} \zeta_m U_{m+1}^{(+)} & \zeta_m V_{m+1}^{(+)} & \zeta_m U_{m+1}^{(-)} & \zeta_m V_{m+1}^{(-)} \\ -\zeta_m R_{m+1}^{(+)} & -\zeta_m S_{m+1}^{(+)} & -\zeta_m R_{m+1}^{(-)} & -\zeta_m S_{m+1}^{(-)} \\ -A_{m+1}^{(+)} & -B_{m+1}^{(+)}-\zeta_{m+1} & -A_{m+1}^{(-)} & -B_{m+1}^{(-)}-\zeta_{m+1} \\ -\eta_y^{m+1}P_{m+1}^{(+)} & -\eta_y^{m+1}Q_{m+1}^{(+)} & -\eta_y^{m+1}P_{m+1}^{(-)} & -\eta_y^{m+1}Q_{m+1}^{(-)} \\ -\zeta_{m+1}U_{m+1}^{(+)} & -\zeta_{m+1}V_{m+1}^{(+)} & -\zeta_{m+1}U_{m+1}^{(-)} & -\zeta_{m+1}V_{m+1}^{(-)} \\ C_{m+1}^{(+)}+\zeta_{m+1} & D_{m+1}^{(+)} & C_{m+1}^{(-)}+\zeta_{m+1} & D_{m+1}^{(-)} \\ +\eta_x^{m+1}P_{m+1}^{(+)} & +\eta_x^{m+1}Q_{m+1}^{(+)} & +\eta_x^{m+1}P_{m+1}^{(-)} & +\eta_x^{m+1}Q_{m+1}^{(-)} \\ +\zeta_{m+1}R_{m+1}^{(+)} & +\zeta_{m+1}S_{m+1}^{(+)} & +\zeta_{m+1}R_{m+1}^{(-)} & +\zeta_{m+1}S_{m+1}^{(-)} \end{bmatrix} \tag{2.36}$$

and the coefficients $P_m^{(\pm)}$, $Q_m^{(\pm)}$ and ζ_m are defined as

$$P_m^{(\pm)}=-\frac{\eta_x^m e^{-\jmath k_x \Delta_x}}{\eta_z^{m(\pm)} e^{\mp \jmath k_z^m \Delta_z^m}} \tag{2.37}$$

$$Q_m^{(\pm)}=-\frac{\eta_y^m e^{-\jmath k_y \Delta_y}}{\eta_z^{m(\pm)} e^{\mp \jmath k_z^m \Delta_z^m}} \tag{2.38}$$

$$\zeta_m=\frac{\Delta t}{\mu_m \Delta_z^m} \tag{2.39}$$

Equation (2.34) can be applied recursively to determine the field coefficients $(E_x^m, E_y^m, E_x^{rm}, E_y^{rm})$ in all the layers $m=1, 2,..., M+1$ in terms of the incident field coefficients (E_x^1, E_y^1) in the uppermost layer $m=1$. To do so, Eq. (2.34) is first rewritten as:

$$\begin{bmatrix} E_x^m \phi_m^{(+)} \\ E_y^m \phi_m^{(+)} \\ E_x^{rm} \phi_m^{(-)} \\ E_y^{rm} \phi_m^{(-)} \end{bmatrix} = [C_m] \begin{bmatrix} E_x^{m+1} \phi_{m+1}^{(+)} \\ E_y^{m+1} \phi_{m+1}^{(+)} \\ E_x^{r(m+1)} \phi_{m+1}^{(-)} \\ E_y^{r(m+1)} \phi_{m+1}^{(-)} \end{bmatrix} \tag{2.40}$$

where

$$[C_m]=[A_m]^{-1}[B_m] \times \begin{bmatrix} e^{\jmath(N_m-N_{m+1}-1)k_z^{m+1}\Delta_z^{m+1}}[I_2] & 0 \\ 0 & e^{-\jmath(N_m-N_{m+1}-1)k_z^{m+1}\Delta_z^{m+1}}[I_2] \end{bmatrix} \tag{2.41}$$

and $[I_2]$ is the 2×2 identity matrix. By repeated application of Eq. (2.40) for $1 \leqslant m \leqslant M$, one obtains

$$\begin{bmatrix} E_x^m \phi_m^{(+)} \\ E_y^m \phi_m^{(+)} \\ E_x^{rm} \phi_m^{(-)} \\ E_y^{rm} \phi_m^{(-)} \end{bmatrix} = [M^{(m)}] \begin{bmatrix} E_x^{M+1} \phi_{M+1}^{(+)} \\ E_y^{M+1} \phi_{M+1}^{(+)} \\ 0 \\ 0 \end{bmatrix} \tag{2.42}$$

where $[M^{(m)}] = \prod_{p=m}^{M} [C_p]$ and it has been assumed that there is no upward propagating wave in the bottommost layer $m = M+1$, so that $E_x^{r(M+1)} = E_y^{r(M+1)} = 0$. Using Eq. (2.42) for $m = 1$, one can solve for the coefficients (E_x^{M+1}, E_y^{M+1}) of the transmitted wave in the bottommost layer and the coefficients (E_x^{r1}, E_y^{r1}) of the reflected wave in the uppermost layer in terms of the incident wave coefficients (E_x^1, E_y^1):

$$\begin{bmatrix} E_x^{M+1} \phi_{M+1}^{(+)} \\ E_y^{M+1} \phi_{M+1}^{(+)} \end{bmatrix} = \begin{bmatrix} M_{11}^{(1)} & M_{12}^{(1)} \\ M_{21}^{(1)} & M_{22}^{(1)} \end{bmatrix}^{-1} \begin{bmatrix} E_x^1 \phi_1^{(+)} \\ E_y^1 \phi_1^{(+)} \end{bmatrix} \tag{2.43}$$

$$\begin{bmatrix} E_x^{r1} \phi_1^{(-)} \\ E_y^{r1} \phi_1^{(-)} \end{bmatrix} = \begin{bmatrix} M_{31}^{(1)} & M_{32}^{(1)} \\ M_{41}^{(1)} & M_{42}^{(1)} \end{bmatrix} \begin{bmatrix} E_x^{M+1} \phi_{M+1}^{(+)} \\ E_y^{M+1} \phi_{M+1}^{(+)} \end{bmatrix} \tag{2.44}$$

Then, by substituting Eq. (2.43) into Eq. (2.42), the field coefficients in the remaining layers $m = 2, \ldots, M$ can be found.

2.3. Numerically Stable Formulation

The iteration scheme based on Eq. (2.42) is numerically stable when the wavevectors k_z^m in the various layers are real. This is the case for lossless layers and propagating, as opposed to evanescent, waves in the various layers. A finite-duration incident pulse traveling in the FDTD lattice, however, usually contains a large number of frequencies, including frequencies so high that the corresponding plane waves are evanescent in the FDTD lattice, as characterized by a complex solution k_z^m to the dispersion relation Eq. (2.8). In such case, the iteration scheme based on Eq. (2.42) can be numerically unstable, especially when the layer thicknesses are large. To overcome this problem, one can adopt the enhanced transmittance-matrix approach used in the rigorous coupled-wave method for electromagnetic diffraction by grating structures [see Moharam *et al.* (1995)]. In this approach, the troublesome term $e^{j(N_m - N_{m+1} - 1) k_z^{m+1} \Delta_z^{m+1}}$ in Eq. (2.41), which increases exponentially rapidly with increasing frequency above the cutoff frequency of the FDTD lattice, is factored out of the matrix $[C_m]$,

$$[C_m] = e^{j(N_m - N_{m+1} - 1) k_z^{m+1} \Delta_z^{m+1}} [\tilde{C}_m] \tag{2.45}$$

where

$$[\tilde{C}_m] = [A_m]^{-1}[B_m]\begin{bmatrix} [I_2] & 0 \\ 0 & e^{-2j(N_m - N_{m+1} - 1)k_z^{m+1}\Delta_z^{m+1}}[I_2] \end{bmatrix} \tag{2.46}$$

This leads to a numerically stable from of Eq. (2.42),

$$\begin{bmatrix} E_x^m \phi_m^{(+)} \\ E_y^m \phi_m^{(+)} \\ E_x^{rm} \phi_m^{(-)} \\ E_y^{rm} \phi_m^{(-)} \end{bmatrix} = e^{j\Phi^m}[\tilde{M}^{(m)}] \begin{bmatrix} E_x^{M+1} \phi_{M+1}^{(+)} \\ E_y^{M+1} \phi_{M+1}^{(+)} \\ 0 \\ 0 \end{bmatrix} \tag{2.47}$$

where $[\tilde{M}^{(m)}] = \prod_{p=m}^{M} [\tilde{C}_p]$ and $\Phi^m = \sum_{p=m}^{M} (N_p - N_{p+1} - 1) k_z^{p+1} \Delta_z^{p+1}$.

3. NUMERICAL RESULTS

The formulation discussed in Section 2 was implemented in a three-dimensional FDTD code for layered, dispersive media. The computational domain consisted of $46 \times 46 \times 46$ FDTD cells. The medium consisted of three layers of different materials separated by horizontal planes coincident with the bottom faces of cells labeled by (i, j, k) with $k = 17$ or $k = 32$. The parameters of the material models were chosen so that the refractive indices of the three layers at a reference wavelength λ_0 were n_1, n_2 and n_3, respectively. The total-field formulation was employed for the computation, in which the scattered-field region consisted of the outermost two layers of FDTD cells in the computational domain. The domain was excited by a finite-duration pulse with arbitrary polarization and direction of incidence, whose waveform was in the shape of the time derivative of a Gaussian pulse,

$$E^{\text{inc}}(n) = -3\sqrt{2e}\left(\frac{n - n_{\text{shift}}}{n_0} - 1\right) e^{-[3((n-n_{\text{shift}})/n_0 - 1)]^2} \tag{3.1}$$

where n_0 is the width of the Gaussian pulse and n_{shift} is the delay, both in units of Δt. Also, the factor $3\sqrt{2e}$ is used to normalize the peak amplitude to unity. The cell dimensions were $\Delta_x = \Delta_y = \Delta_z^m = 1$ unit and Δt was chosen so that $c\,\Delta t = 0.5$ unit, where c is the velocity of light in free space. For simplicity, the first-order Higdon absorbing boundary condition [Higdon (1986)] was used on all six sides of the computational domain.

The incident pulse Eq. (3.1) was decomposed into various Fourier components with frequencies ω_i and amplitudes f_i, $i = 1, \ldots, N$, where N is the sample size for waveform synthesis by Fast Fourier Transform (FFT). In order to represent an incident pulse propagating in a well-defined direction (θ, ϕ), the incident plane waves corresponding to the various Fourier

components were all assumed to have the same transverse wavevector $(k_x, k_y) = (k_0 \sin\theta \cos\phi, k_0 \sin\theta \sin\phi)$, where $k_0 = 2\pi/\lambda_0$ and $\lambda_0 = 15.7$ units. Furthermore, all such plane-wave components of the incident pulse were assumed to have the same polarization, which could be TE or TM. In the former case, the y component of the incident electric field vanishes, while in the latter case, the y component of the incident magnetic field vanishes.

For each plane-wave component of the incident pulse, the steady-state field distribution in the FDTD lattice in the absence of a scatterer was computed using the analytical procedure discussed in Section 2. The result in each cell on the fictitious excitation surface S was saved. Then, the stored steady-state results at each cell of S were weighted by their corresponding Fourier amplitudes f_i and the resulting time-domain waveform was synthesized by FFT. This time-domain waveform represents the incident wave in the FDTD lattice in the absence of a scatterer. Using the same procedure, the time-domain waveform of the incident wave over an observation plane $j = 26$, which passes through the middle of the FDTD lattice, was also computed analytically for comparison with the FDTD results.

In each test example, the absolute values of the dominant component of the total electric field, namely, E_x or E_y for TE or TM polarization, respectively, in cells on the observation plane $j = 26$ and lying within the total-field region were recorded at each time step n. These values were averaged over all such cells to obtain an estimate of the average magnitude of the dominant component of the electric field in the total-field region of the computational domain at each time step n. Next, the absolute value of the *difference* between the value of the dominant electric field component computed by FDTD and the value obtained previously using the analytical procedure was found for each cell with $j = 26$ and lying within the total-field region, at each time step n. These values were averaged over the same cells to obtain an estimate of the discrepancy between the FDTD and the analytical results in the total-field region at each time step n. Lastly, the absolute values of the dominant electric field component in cells with $j = 26$ and lying in the scattered-field region were recorded and averaged over the same cells, at each time step n. This gave an estimate of the residual error in the cancellation of the FDTD computed fields outside the excitation surface S by the analytically computed incident fields applied to S.

Figure 4 shows the results for the lossless dielectric case, with $n_1 = 1.5$, $n_2 = 2.0$ and $n_3 = 1.0$. The incident pulse parameters were $n_0 = 44$, $n_{\text{shift}} = 80$, $(\theta, \phi) = (179.9°, 3.04°)$ and TE polarization. A sample size of $N = 2048$ was used for waveform synthesis by FFT. The solid curve shows the average magnitude of E_x over the observation plane $j = 26$ in the total-field region, as a function of the time step n. The dashed curve shows the

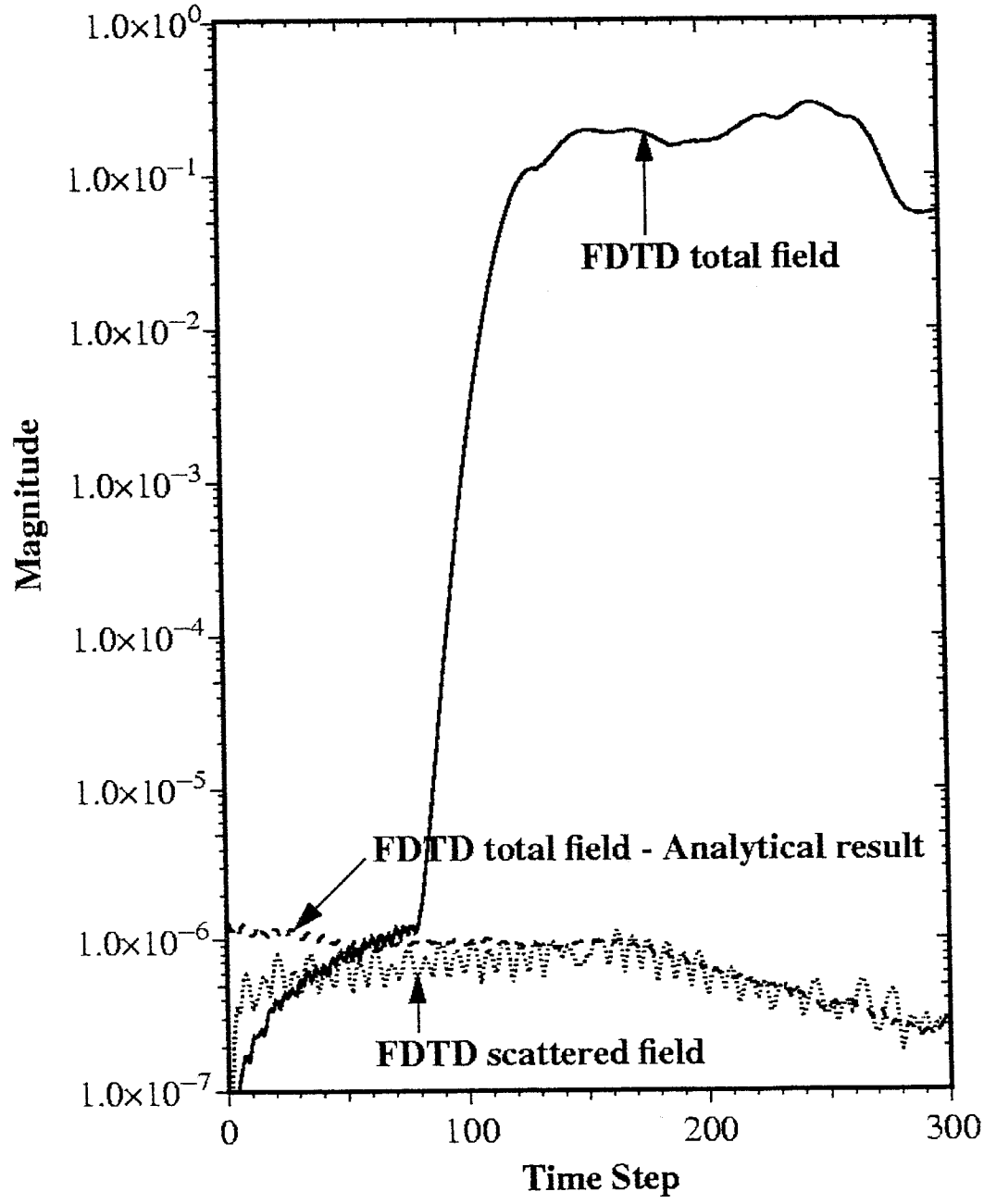

Fig. 4. Comparison between FDTD fields and the analytical results for a layered, lossless medium, on an observation plane perpendicular to the Y axis. $n_1 = 1.5$, $n_2 = 2.0$, $n_3 = 1.0$. $(\theta, \phi) = (179.9°, 3.04°)$.

ayered, lossless
$= 2.0$, $n_3 = 1.0$.

average magnitude of the discrepancy between the FDTD and analytical results over the plane $j = 26$ in the total-field region, as a function of n. The dotted curve shows the average magnitude of the residual field over the plane $j = 26$ in the scattered-field region. From the solid curve in Fig. 4, the electric field in the total-field region is seen to start from a very small value at $n = 1$, rise after a delay of about 80 time steps to a peak average magnitude of about 0.3 and then decay as the finite-duration incident wave eventually passed out of the computational domain. Even though the incident pulse given by Eq. (3.1) had a width n_0 of only 44 time steps, the incident wave in the FDTD lattice extended over a much longer interval of several hundred time steps, due to the multiple reflections occurring within the layered lattice. From the dashed curve in Fig. 4, however, the discrepancy between the FDTD and analytical results for the total electric field started at a magnitude of about 10^{-6} and remained at or below this value for all time steps n. Most of this discrepancy can be attributed to FFT aliasing, since the sample size of $N = 2048$ used for the FFT was barely large enough to synthesize accurately an incident waveform lasting several hundred time steps. Thus, whereas the FDTD fields were initialized to zero at $n = 0$, the analytically computed fields in the total-field region were already found to have a magnitude of about 10^{-6} at $n = 1$ due to FFT aliasing. This aliasing error can be reduced by using a larger sample size N for waveform synthesis, but at the expense of increased computer storage requirement. By comparing the solid and dashed curves in Fig. 4, one can conclude that the difference between the analytically computed fields and the FDTD fields in the total-field region was negligible except for the FFT aliasing error. Furthermore, from the dotted curve in Fig. 4, one can conclude that the analytically computed incident fields applied to the excitation surface S produced a null field in the scattered-field region to about the same accuracy, limited only by FFT aliasing error.

The results for the case of lossy, dispersive materials are shown in Fig. 5, with $n_1 = 1.5 - 0.5j$, $n_2 = 1.0 - 1.5j$, $n_3 = 1.0$, $(\theta, \phi) = (143.8°, 34.3°)$ and TM polarization. n_0, n_{shift} and N were the same as in Fig. 4. Layer 1 was modeled by a conducting material and layer 2 by an unmagnetized plasma as discussed in the Appendix. The dashed curve in Fig. 5 shows the presence of FFT aliasing error of about 0.6×10^{-6} or less in magnitude. This means that the difference between the FDTD and analytically computed fields in the total-field region was negligible except for FFT aliasing error. Furthermore, the dotted curve in Fig. 5 shows that the analytically computed incident fields applied to S produced a null field in the scattered-field region to about the same accuracy, limited only by FFT aliasing error.

Figure 6 illustrates these observations in a different way. Here, the magnitude of the FDTD computed electric field component E_y on an

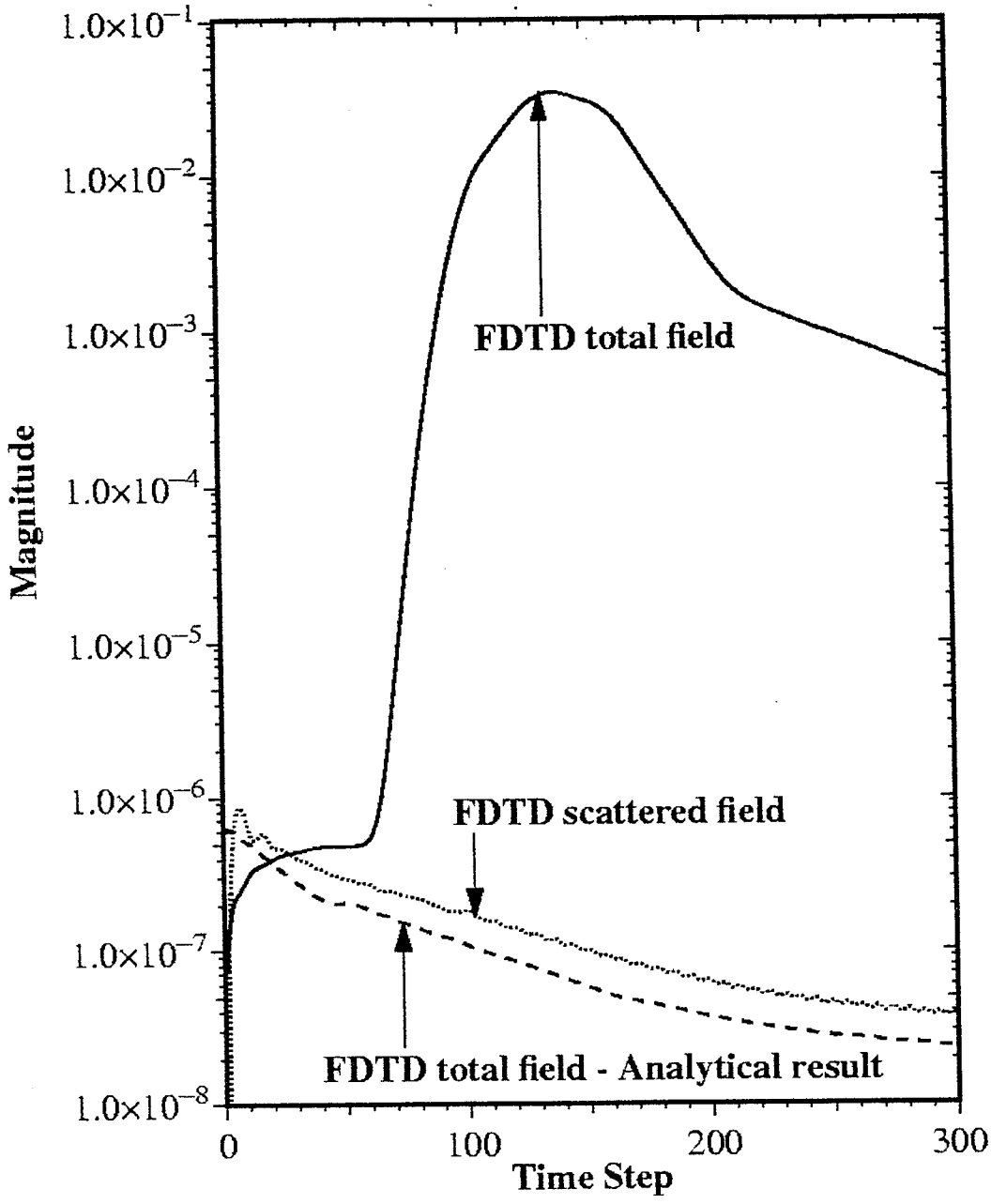

Fig. 5. Comparison between FDTD fields and the analytical results for a layered, lossy and dispersive medium, on an observation plane perpendicular to the Y axis. $n_1 = 1.5 - 0.5j$, $n_2 = 1.0 - 1.5j$, $n_3 = 1.0$ at the center wavelength of the incident pulse. $(\theta, \phi) = (143.8°, 34.3°)$.

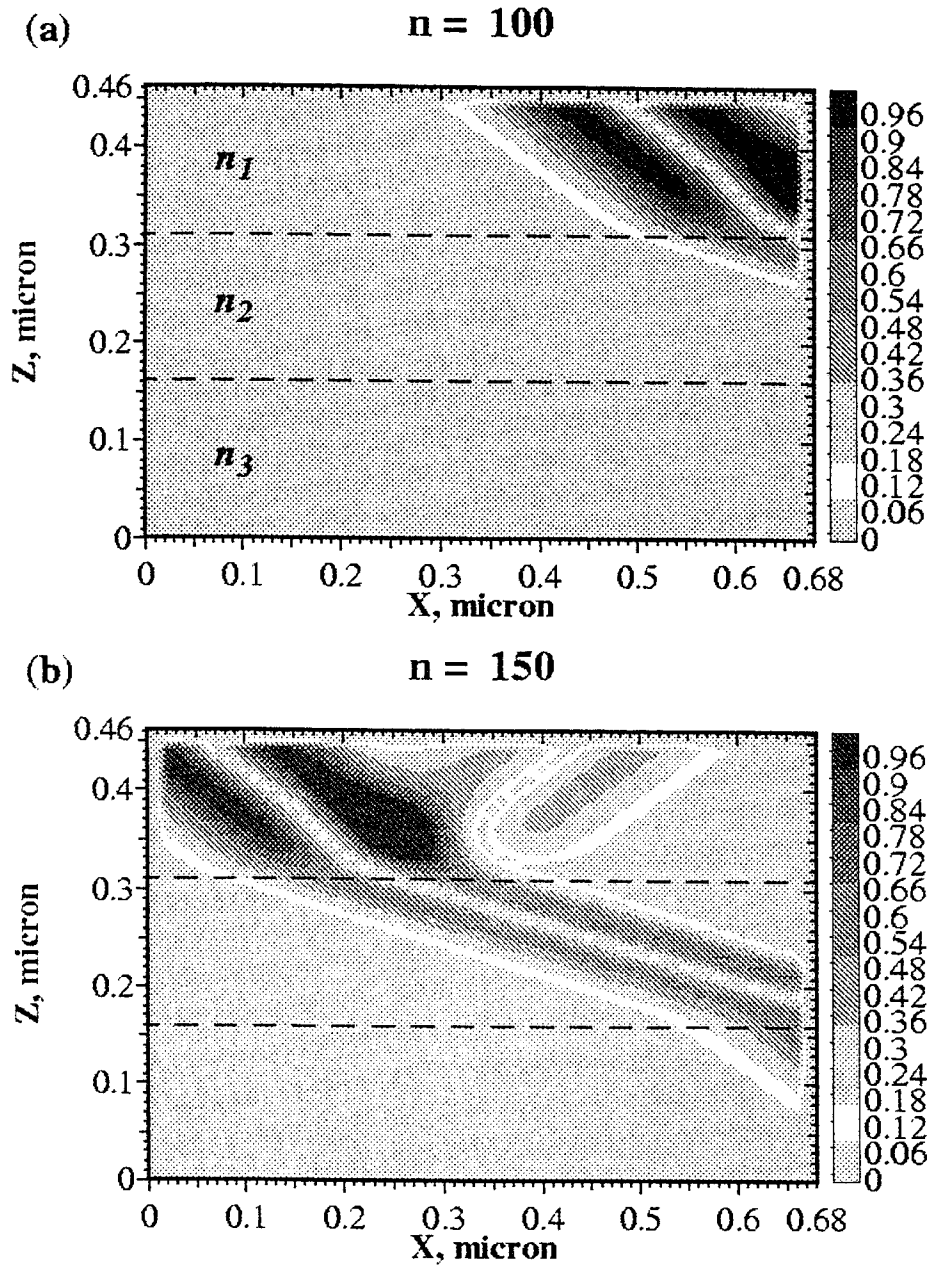

Fig. 6. Field computed by FDTD on an observation plane perpendicular to the Y axis. $n_1 = 1.0$, $n_2 = 2.0$, $n_3 = 1.0$. $(\theta, \phi) = (143.8°, 3.04°)$. The dotted lines mark the interfaces between adjacent layers. Only the magnitude of E_y is shown. (a) $n = 100$: The two peaks of the incident pulse are seen to enter the computational domain from the upper right corner; (b) $n = 150$: The transmitted wave in the middle layer and the reflected wave in the top layer are visible; (c) $n = 200$: The transmitted wave in the bottom and both the transmitted and reflected waves in the middle layer are visible; (d) $n = 250$: The reflected wave in the middle layer is seen to propagate into the top layer. At all time steps, the scattered-field region, represented by the thin white border just inside the boundaries of the computational domain, had negligible field due to the absence of a scattering object.

observation plane perpendicular to the Y axis at various time steps is shown. The layers were lossless to allow clear observation of the multiply reflected waves in the layered FDTD lattice. The parameters were $n_1 = 1.0$, $n_2 = 2.0$, $n_3 = 1.0$, $(\theta, \phi) = (143.8°, 3.04°)$, $n_0 = 33$, $n_{\text{shift}} = 80$ and the polarization was TM. In Fig. 6, the incident wave is seen to enter the computational domain from the upper right corner, undergo multiple reflections in

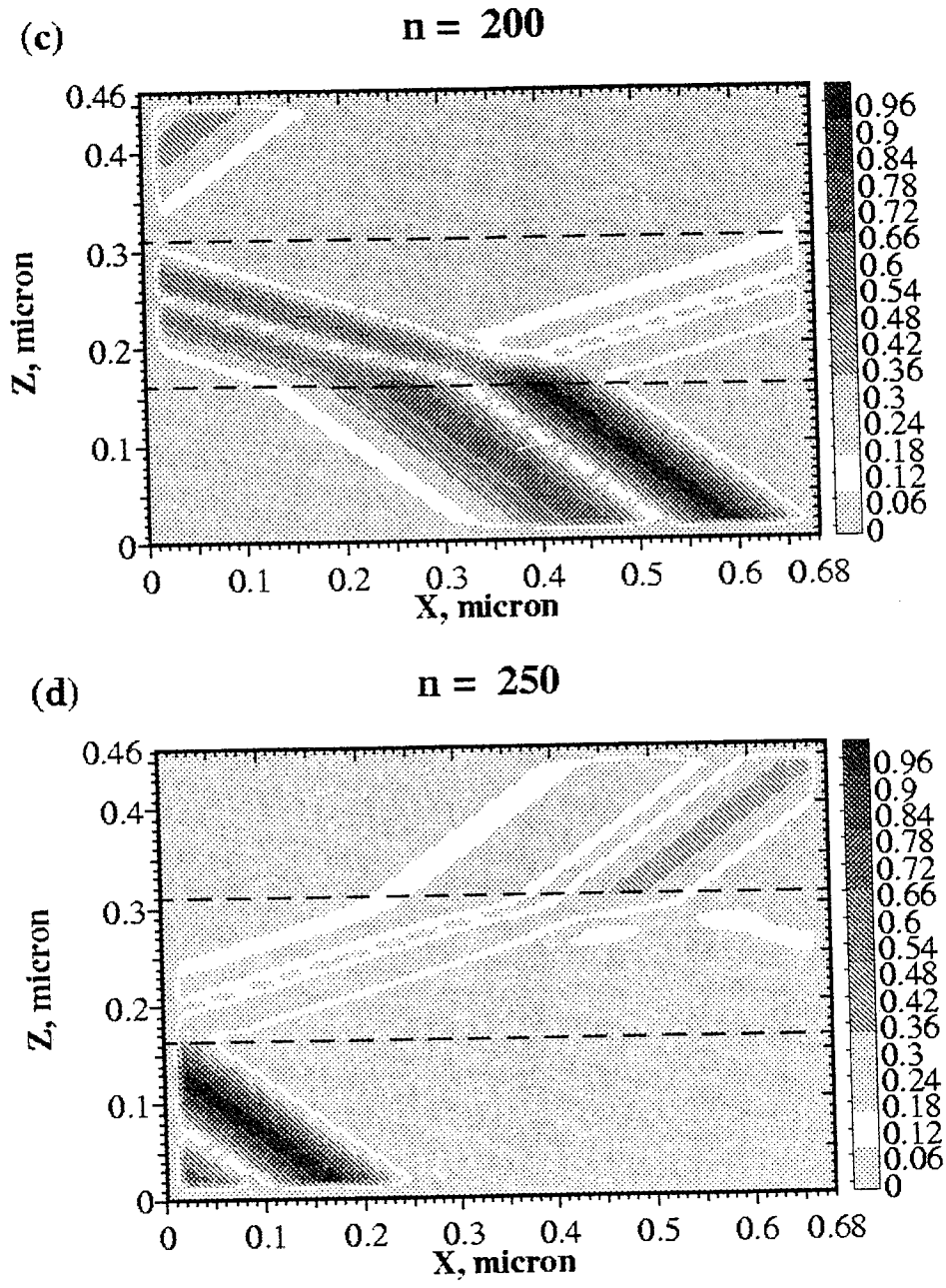

Fig. 6. (*Continued*)

the layered FDTD lattice and eventually pass out of the computational domain. At the same time, the outermost two FDTD layers of the computational domain representing the scattered-field region had negligible fields at all time steps due to the nearly perfect cancellation of the incident wave outside the fictitious excitation surface.

4. CONCLUSIONS

In this paper, an incident wave source for FDTD electromagnetic computations involving layered dispersive media has been described. The wave source can in principle generate an arbitrary incident wave obeying the dispersion relations and reflection and transmission relations of the layered FDTD lattice exactly. In practical computation, a small amount of FFT aliasing error, on the order of 10^{-5} times the peak amplitude of the incident pulse, is usually present in the incident fields generated by the wave source. This source of error can be reduced by increasing the sample size for FFT waveform synthesis, but at the expense of increased computer storage requirement.

APPENDIX

In this Appendix, the electric field updating equations for a plane wave of the form

$$\begin{bmatrix} E^n_{x,\,i+1/2,\,j,\,k} \\ E^n_{y,\,i,\,j+1/2,\,k} \\ E^n_{z,\,i,\,j,\,k+1/2} \\ H^{n+1/2}_{x,\,i,\,j+1/2,\,k+1/2} \\ H^{n+1/2}_{y,\,i+1/2,\,j,\,k+1/2} \\ H^{n+1/2}_{z,\,i+1/2,\,j+1/2,\,k} \end{bmatrix} = \begin{bmatrix} E^m_x \\ E^m_y \\ E^m_z \\ H^m_x \\ H^m_y \\ H^m_z \end{bmatrix} e^{j\omega n\,\Delta t - j(ik_x\,\Delta_x + jk_y\,\Delta_y - kk^m_z\,\Delta^m_z)} \tag{A.1}$$

traveling in an FDTD layer modeled by one of several material models are derived.

A.1. Conducting Material

Starting from Maxwell's equation for $\partial E_x/\partial t$ in a conducting medium with parameters (ε, σ),

$$\varepsilon \frac{\partial E_x}{\partial t} + \sigma E_x = \frac{\partial H_z}{\partial y} - \frac{\partial H_y}{\partial z} \tag{A.2}$$

one obtains the FDTD version of Eq. (A.2) by applying the Yee algorithm,

$$\varepsilon \frac{E^{n+1}_{x,\,i+1/2,\,j,\,k} - E^{n}_{x,\,i+1/2,\,j,\,k}}{\Delta t} + \sigma \frac{E^{n+1}_{x,\,i+1/2,\,j,\,k} + E^{n}_{x,\,i+1/2,\,j,\,k}}{2}$$
$$= \frac{H^{n+1/2}_{z,\,i+1/2,\,j+1/2,\,k} - H^{n+1/2}_{z,\,i+1/2,\,j-1/2,\,k}}{\Delta_y} - \frac{H^{n+1/2}_{y,\,i+1/2,\,j,\,k+1/2} - H^{n+1/2}_{y,\,i+1/2,\,j,\,k-1/2}}{\Delta^m_z} \tag{A.3}$$

By substituting Eq. (A.1) into Eq (A.3) and simplifying, one obtains

$$\varepsilon E^m_x \left[\left(1 + \frac{\sigma\,\Delta t}{2\varepsilon} \right) e^{j\omega\,\Delta t} - \left(1 - \frac{\sigma\,\Delta t}{2\varepsilon} \right) \right]$$
$$= \Delta t \left[\frac{1 - e^{jk_y \Delta_y}}{\Delta_y} H^m_z - \frac{1 - e^{-jk^m_z \Delta^m_z}}{\Delta^m_z} H^m_y \right] \tag{A.4}$$

Comparing Eqs. (A.4) and (2.2), one obtains

$$\varepsilon_m = \varepsilon \tag{A.5}$$

$$\gamma_m = 1 + \frac{\sigma\,\Delta t}{2\varepsilon} \tag{A.6}$$

$$\beta_m = 1 - \frac{\sigma\,\Delta t}{2\varepsilon} \tag{A.7}$$

A.2. Unmagnetized Plasma

Maxwell's equation for $\partial D_x/\partial t$ in an unmagnetized plasma characterized by an electric susceptibility $\chi(t)$,

$$\chi(t) = \frac{\omega_p^2}{\nu_c} (1 - e^{-\nu_c t})\, U(t) \tag{A.8}$$

$U(t)$ being the unit step function, is

$$\frac{\partial D_x}{\partial t} = \frac{\partial H_z}{\partial y} - \frac{\partial H_y}{\partial z} \tag{A.9}$$

where

$$D_x(t) = \varepsilon_0 E_x(t) + \varepsilon_0 \int_0^\infty \chi(\tau)\, E_x(t - \tau)\, d\tau \tag{A.10}$$

algorithm,

Substituting Eq. (A.8) into Eq. (A.10) and taking the time derivative of both sides of the latter equation, one obtains

$$\frac{\partial D_x}{\partial t} = \varepsilon_0 \frac{\partial E_x}{\partial t} + \varepsilon_0 \int_0^\infty \omega_p^2 e^{-\nu_c \tau} E_x(t-\tau)\, d\tau \tag{A.11}$$

1/2
+ 1/2, j, k − 1/2

(A.3)

where an integration by parts has been performed, assuming that $E_x(t)$ vanishes as t approaches $-\infty$. To evaluate the convolution integral in Eq. (A.11), the electric field $E_x(t)$ is assumed to have the value $E_x(n)$ at time step n and to vary linearly between successively time steps. Thus, for $m = 0, 1, \ldots,$

(A.4)

$$E_x(t-\tau) \approx E_x(n-m) + [E_x(n-m-1) - E_x(n-m)] \frac{\tau - m\,\Delta t}{\Delta t}$$

$$\text{for} \quad m\,\Delta t \leqslant \tau < (m+1)\,\Delta t \tag{A.12}$$

(A.5)

where $t = n\,\Delta t$ and the spatial indices have been omitted for simplicity. This way, the convolution integral can be evaluated,

(A.6)

$$\int_0^\infty \omega_p^2 e^{-\nu_c \tau} E_x(t-\tau)\, d\tau = \sum_{m=0}^{\infty} \int_{m\,\Delta t}^{(m+1)\,\Delta t} \omega_p^2 e^{-\nu_c \tau} E_x(t-\tau)\, d\tau$$

(A.7)

$$\approx \omega_p^2\, \Delta t \left[\alpha_0 E_x(n) + \alpha_1 \sum_{m=1}^{\infty} e^{-\nu_c m\,\Delta t} E_x(n-m) \right] \tag{A.13}$$

sma charac-

where $t = n\,\Delta t$ and α_0 and α_1 are given by

(A.8)

$$\alpha_0 = \frac{1}{\nu_c\,\Delta t}\left[1 - \left(\frac{1 - e^{-\nu_c\,\Delta t}}{\nu_c\,\Delta t}\right)\right] \tag{A.14}$$

$$\alpha_1 = 2\left[\frac{\cosh(\nu_c\,\Delta t) - 1}{(\nu_c\,\Delta t)^2}\right] \tag{A.15}$$

(A.9)

Using the fact that, for the plane wave of Eq. (A.1), $E_x(n)$ is proportional to $e^{jn\omega\,\Delta t}$, the summation in Eq. (A.13) can be evaluated. Thus,

(A.10)

$$\int_0^\infty \omega_p^2 e^{-\nu_c \tau} E_x(t-\tau)\, d\tau \approx \omega_p^2\, \Delta t\, E_x(n) \left[\alpha_0 + \frac{\alpha_1}{e^{(j\omega + \nu_c)\,\Delta t} - 1}\right] \tag{A.16}$$

where $t = n\,\Delta t$. Substituting Eq. (A.16) into Eq. (A.11) and making the finite-difference approximation, one obtains

$$\left.\frac{\partial D_x}{\partial t}\right|^{n+1/2} \approx \varepsilon_0 \frac{E_x(n+1)-E_x(n)}{\Delta t} + \varepsilon_0 \omega_p^2\,\Delta t\, E_x\left(n+\frac{1}{2}\right)\left[\alpha_0 + \frac{\alpha_1}{e^{(j\omega+\nu_c)\,\Delta t}-1}\right]$$

$$\approx \varepsilon_0 E_x(n)\left\{\frac{e^{j\omega\,\Delta t}-1}{\Delta t} + \frac{\omega_p^2\,\Delta t}{2}\left(e^{j\omega\,\Delta t}+1\right)\left[\alpha_0 + \frac{\alpha_1}{e^{(j\omega+\nu_c)\,\Delta t}-1}\right]\right\} \tag{A.17}$$

where $t = (n+\frac{1}{2})\,\Delta t$ and $E_x(n+\frac{1}{2})$ has been approximated by $\frac{1}{2}[E_x(n+1)+E_x(n)]$. By substituting Eq. (A.17) into the LHS of Eq. (A.9) and using the Yee finite-difference approximation for the RHS of the latter equation, one obtains,

$$\varepsilon_0 E_x^m \left\{\left(e^{j\omega\,\Delta t}-1\right) + \frac{(\omega_p\,\Delta t)^2}{2}\left(e^{j\omega\,\Delta t}+1\right)\left[\alpha_0 + \frac{\alpha_1}{e^{(j\omega+\nu_c)\,\Delta t}-1}\right]\right\}$$

$$= \Delta t\left[\frac{1-e^{jk_y\,\Delta_y}}{\Delta_y} H_z^m - \frac{1-e^{-jk_z^m\,\Delta_z^m}}{\Delta_z^m} H_y^m\right] \tag{A.18}$$

where $E_x(n)$ has been identified with $E^n_{x,\,i+1/2,\,j,\,k}$ and Eq. (A.1) has been used. Comparing Eqs. (A.18) and (2.2), one obtains

$$\varepsilon_m = \varepsilon_0 \tag{A.19}$$

$$\gamma_m = 1 \tag{A.20}$$

$$\beta_m = 1 - \frac{(\omega_p\,\Delta t)^2}{2}\left(e^{j\omega\,\Delta t}+1\right)\left[\alpha_0 + \frac{\alpha_1}{e^{(j\omega+\nu_c)\,\Delta t}-1}\right] \tag{A.21}$$

A.3. Lorentz Material

The electric susceptibility for a Lorentz material is

$$\chi(t) = \frac{(\varepsilon_s-\varepsilon_0)\,\omega_0^2}{\sqrt{\omega_0^2-\delta^2}}\,\mathrm{Im}(e^{-\gamma t})\,U(t)$$

$$= \frac{(\varepsilon_s-\varepsilon_0)\,\omega_0^2}{2j\sqrt{\omega_0^2-\delta^2}}\left(e^{-\gamma t}-e^{-\gamma^* t}\right)U(t) \tag{A.22}$$

making the

$$\frac{\alpha_1}{\omega+\nu_c)\,\Delta t-1}\Bigg]$$

$$\frac{1}{\nu_c)\,\Delta t-1}\Bigg]\Bigg\}$$

(A.17)

timated by
of Eq. (A.9)
of the latter

$$\frac{}{-1}\Bigg]\Bigg\}$$

(A.18)

A.1) has been

(A.19)

(A.20)

$$\Bigg]$$

(A.21)

(A.22)

where ε_s, ω_0 and δ are real constants and $\gamma = \delta - \hat{\jmath}\sqrt{\omega_0^2 - \delta^2}$. Following the procedure leading from Eq. (A.10) to Eq. (A.17), one obtains

$$\left.\frac{\partial D_x}{\partial t}\right|^{n+1/2} \approx \varepsilon_0 E_x(n)\left\{\frac{e^{\hat{\jmath}\omega\,\Delta t}-1}{\Delta t} - \frac{(\varepsilon_s-\varepsilon_0)\,\omega_0^2\,\Delta t}{4\hat{\jmath}\sqrt{\omega_0^2-\delta^2}}\,(e^{\hat{\jmath}\omega\,\Delta t}+1)\right.$$
$$\left.\times\left[\gamma\tilde{\alpha}_0 - (\gamma\tilde{\alpha}_0)^* + \frac{\gamma\tilde{\alpha}_1}{e^{(\hat{\jmath}\omega+\gamma)\,\Delta t}-1} - \frac{(\gamma\tilde{\alpha}_1)^*}{e^{(\hat{\jmath}\omega+\gamma^*)\,\Delta t}-1}\right]\right\} \tag{A.23}$$

where $\tilde{\alpha}_0$ and $\tilde{\alpha}_1$ are given by

$$\tilde{\alpha}_0 = \frac{1}{\gamma\,\Delta t}\left[1 - \left(\frac{1-e^{-\gamma\,\Delta t}}{\gamma\,\Delta t}\right)\right] \tag{A.24}$$

$$\tilde{\alpha}_1 = \left[\frac{e^{\gamma\,\Delta t} + e^{-\gamma\,\Delta t} - 2}{(\gamma\,\Delta t)^2}\right] \tag{A.25}$$

By comparing Eqs. (A.23) and (A.17), one finds that the only difference between the unmagnetized plasma and the Lorentz material is that the β_m of Eq. (A.21) for the unmagnetized plasma is replaced by

$$\beta_m = 1 - j\frac{(\varepsilon_s-\varepsilon_0)(\omega_0\,\Delta t)^2}{4\sqrt{\omega_0^2-\delta^2}}\,(e^{\hat{\jmath}\omega\,\Delta t}+1)$$
$$\times\left[\gamma\tilde{\alpha}_0 - (\gamma\tilde{\alpha}_0)^* + \frac{\gamma\tilde{\alpha}_1}{e^{(\hat{\jmath}\omega+\gamma)\,\Delta t}-1} - \frac{(\gamma\tilde{\alpha}_1)^*}{e^{(\hat{\jmath}\omega+\gamma^*)\,\Delta t}-1}\right] \tag{A.26}$$

for the Lorentz material.

ACKNOWLEDGMENT

This research was supported by a MURI grant from AFOSR and DARPA.

REFERENCES

Higdon, R. L. (1986). Absorbing boundary conditions for difference approximations to the multidimensional wave equation, *Math. Comput.* **47**, 437–459.

Holland, R., and Williams, J. W. (1983). Total-field versus scattered-field finite-difference codes: A comparative assessment, *IEEE Trans. Nuclear Sci.* **NS-30**, 4583–4588.

Moharam, M. G., Pommet, D. A., and Grann, E. B. (1995). Stable implementation of the rigorous coupled-wave analysis for surface-relief gratings: Enhanced transmittance matrix approach, *J. Opt. Soc. Amer.* **A12**, 1077–1086.

Taflove, A. (1995). *Computational Electrodynamics the Finite-Difference Time-Domain Method*, Artech House, Boston.

Yee, K. S. (1966). Numerical solution of initial boundary value problems involving Maxwell's equations in isotropic media, *IEEE Trans. Antennas Propagat.* **AP-14**, 302–307.